An Automated Gradient Titration Fluorescence Methodology for High-Resolution Identification of Aqueous Two-Polymer Phase Extraction Conditions for Single-Wall Carbon Nanotubes

Christopher M. Sims* and Jeffrey A. Fagan

Materials Science and Engineering Division
National Institute of Standards and Technology, Gaithersburg, MD USA 20899

ORCID
Christopher M. Sims: 0000-0002-5623-6974
Jeffrey A. Fagan: 0000-0003-1483-5554

*Corresponding author: Tel: 301-975-2671. E-mail: christopher.sims@nist.gov (Christopher Sims)

Keywords
Single-wall carbon nanotube; SWCNT; aqueous two-phase extraction; separation

Abstract

A significant advance in rate and precision of identifying the co-surfactant concentrations leading to differential extraction of specific single-wall carbon nanotube (SWCNT) species in aqueous two-polymer phase extraction experiments is reported. These gains are achieved through continuous titration of co-surfactant and other solution components during automated fluorescence measurements on SWCNT dispersions. The resulting fluorescence *versus* concentration curves display intensity and wavelength shift transitions traceable to the nature of the adsorbed surfactant layer on specific SWCNT structures at the (*n*,*m*) species and enantiomer level at high resolution. The increased precision and speed of the titration method resolve previously invisible complexity in the SWCNT fluorescence during the transition from one surfactant dominating the SWCNT interface to the other, offering insight into the fine details of the competitive exchange process. For the first time, we additionally demonstrate that the competitive process of the surfactant switch is direction independent (reversible) and hysteresis-free; the latter data effectively specifies an upper bound for the time scale of the exchange process. Titration

curves are compared to literature results and initial advanced parameter variation is conducted for previously unreasonable to investigate solution conditions.

1. Introduction

Competitive binding of two or more surfactants in the presence or absence of multiple other solution components is the basis for several manners of single-wall carbon nanotube (SWCNT) species separation [1, 2], including density gradient ultracentrifugation [3, 4], gel chromatography [5, 6], and aqueous two-polymer phase extraction (ATPE) [7-9]. Originally developed for the separation of bioparticles [10, 11], ATPE leverages the spinodal decomposition of an aqueous solution of polymers into two phases, each with a differential affinity for the dispersed SWCNTs. In common ATPE separations, SWCNT species covered with an adsorbed layer of a bile salt surfactant are selectively partitioned to a dextran (DEX)-rich polymer phase, and SWCNT species with an adsorbed layer dominated by sodium dodecyl sulfate (SDS) partition to a polyethylene glycol (PEG)-rich polymer phase [12-14]. Each SWCNT species, and even enantiomeric handedness, has previously been found to display an abrupt shift in its dominant adsorbed surfactant at specific ratios of surfactant concentrations, which appears to be the underlying mechanism behind the selective SWCNT partitioning in ATPE [15, 16].

Previous work has shown the optical properties of SWCNT species are strongly influenced by their surrounding environment [17-19], such as differences in the composition and packing structure of adsorbed surfactants on the SWCNT surface. For semiconducting SWCNT species, which fluoresce, both the emission peak intensity and location are dependent on the dominant surfactant, with bile salt covered SWCNTs generally displaying brighter fluorescence than the same SWCNTs covered by SDS [20, 21]. Recently, we demonstrated the use of single-phase near-infrared (NIR) fluorescence measurements to monitor the emission intensity of various SWCNT species as a function of the SDS-bile salt surfactant ratio, enabling direct quantification of solution conditions that select for PEG-phase extraction of various (*n,m*) species without conducting physical ATPE separations, which we termed as partition coefficient change conditions (PCCCs) [22]. This methodology development enabled us to conduct faster quantitative evaluations of ATPE experimental parameters, such as temperature, polymer concentration, and surfactant chemistry, on these PCCCs for several (*n,m*) SWCNTs [16, 22], leading to improved understanding of the governing principles behind the ATPE method.

While these reports yielded significant progress towards optimizing ATPE systems for isolation of individual (*n,m*) SWCNT species and their enantiomers, the phase space of possible systematic variations in ATPE separations is extremely large. Despite the recent improvements in measurement speed and

quantitation, it is still difficult to investigate the many possible variations in surfactant chemistry, combinations of surfactants, addition of components such as salts or oxidants, or other factors including pH and temperature, that might yield improved SWCNT separations [16, 23-28]. As such, there is a need for even faster and more precise approaches for screening different ATPE systems for SWCNT separations.

In this contribution, we detail the development and evaluation of a new automated gradient titration method for determining SWCNT PCCCs *via* NIR fluorescence spectroscopy. By incorporating an automated titration system into our existing fluorescence monitoring methodology, we succeed in increasing both the measurement throughput and data resolution by over a factor of 5, while vastly reducing the quantity of SWCNT sample needed for experiments. While significant in of themselves, these measurement enhancements also reveal previously unseen fluorescence phenomena during the surfactant exchange process, with correlative probing of SWCNT-surfactant interactions. We additionally present results of initial screening of complex ATPE systems, such as multi-surfactant mixtures and monovalent electrolyte additions, demonstrating the ability to rapidly identify new ATPE mixtures that may better isolate difficult to separate (*n,m*) species and their handed enantiomers. This methodology advance has massive potential for accelerating SWCNT separations development and facilitating SWCNT technologies.

2. Materials and Methods

Certain equipment, instruments, software, or materials, commercial or non-commercial, are identified in this paper in order to specify the experimental procedure adequately. Such identification is not intended to imply recommendation or endorsement of any product or service by the National Institute of Standards and Technology (NIST), nor is it intended to imply that the materials or equipment identified are necessarily the best available for the purpose.

The SWCNT populations utilized in this work were prepared similarly to those of previous reports [7-9]. In brief, samples were purified from tip sonication-based dispersions followed by liquid-phase processing of SWCNTs synthesized *via* the cobalt-molybdenum-catalyst (CoMoCat) synthesis method (CG400 grade, Chasm Nanotechnologies, USA) or high-pressure CO disproportiation (HiPCO) synthesis method (NoPo Nanotechnologies). Polyethylene glycol (PEG, 6 kDa) was acquired from Alfa Aesar.

Sodium dodecyl sulfate (SDS, BioXtra grade, ≥ 99 %), sodium deoxycholate (DOC, BioXtra ≥ 98 %), sodium cholate (SC, BioUltra, ≥ 99 %), and sodium thiocyanate (NaSCN, ACS Reagent, ≥ 98.0 %) were purchased from Sigma-Aldrich. Sodium chloride (NaCl, ACS Reagent grade, ≥ 99 %) was acquired from VWR. Cesium chloride (CsCl, 99.99 % metals basis) was acquired from Alfa Aesar. All salts, and PEG polymer and surfactant powders were used as received. Ultrapure water (18 MΩ·cm resistivity, Barnstead MicroPure, Thermo Scientific) was used in the preparation of all solutions.

Briefly, SWCNT dispersions were formed by tip sonication (30 min, 93 % amplitude yielding ≈ 1 W/mL, in an ice bath) of received soot at a concentration of 1 mg/mL in a solution of 20.0 g/L DOC in H_2O. Each dispersion was then subjected to a multistep purification series including centrifugation, rate-zonal centrifugation and ATPE separation as described in prior work [29]. Stirred ultrafiltration cells (Millipore) were used to iteratively remove solution components (*e.g.*, iodixanol, ATPE polymers) and to concentrate and exchange *via* back dilution the SWCNT populations into set surfactant solution concentrations such as to 10.0 g/L (1.0 % mass/volume) DOC.

Absorbance spectra were measured on a Cary 5000 UV-visible-near infrared (UV-vis-NIR) absorbance spectrophotometer through a 1 mm path length cuvette at room temperature. Samples and reference solutions were measured in separate runs and the reference spectra subtracted during data analysis. Measurements were conducted for the range of 200 nm to 1400 nm with a 1 nm step, a 2 nm bandpass, and an integration time of 0.1 s/step.

Near-infrared (NIR) fluorescence of the samples was measured in an NS3 Nanospectralyzer (Applied NanoFluorescence), with multiple laser wavelength excitation capabilities [(404, 532, 637, 671, and 782) nm]. For fluorescence-titration experiments, stock SWCNT dispersions were diluted with appropriate additions of the polymer and co-surfactant solutions to reach the specified starting surfactant concentrations of each measurement. A known volume (800 μL) of SWCNT solution was then added to a water-jacketed 10 mm path length fluorescence cuvette (Firefly Science) and the titration apparatus and stirrer (Spectrocell) attached. The titration apparatus consists of a titrant-filled plastic syringe (BD) with Luer-Lok attached polyethylene tubing (Scientific Commodities) controlled by a syringe pump (Braintree Scientific). During measurements, the temperature of the sample within the instrument was controlled to (20.0 ± 0.2) °C using the water-jacketed cuvette attached to a temperature monitored water reservoir (PolyScience). The flowrate from the reservoir through the cell as driven by a small pump

was measured at ≈ 100 mL/min and was verified to be sufficient to maintain the temperature of the liquid in the cell at the set point throughout all measurements. Titration of the surfactant and other solution components was achieved using the syringe pump to add to the total volume of liquid in the sample cuvette at set rates; addition rates were set at 20 μL/min unless otherwise specified. A maximum titrant volume addition equal to the starting dispersion volume (800 μL) was used to maintain a constant final dilution factor of 2. Each titrant solution was constructed to maintain all other solution components at constant concentration during titration, *e.g.*, fixed bile salt and polymer concentration. Typical values unless otherwise specified were 0.5 g/L (0.05 %) DOC, and 35 g/L (3.5 %) 6 kDa PEG; these conditions will be referred to in the text as "standard conditions". Our previous work has shown that using this 6 kDa PEG concentration in fluorescence measurements resulted in very strong agreement to the PCCCs from physical ATPE separations under typical conditions, which is thought to be the PEG concentration experienced by SWCNTs residing in the DEX phase immediately before partitioning to the PEG layer in the overall ATPE microphase separation [16, 22]. A new syringe was used for each titrant and the titration tubing was flushed several times with water when preparing a new titrant for experiments. The cuvette was likewise rinsed with water several times between each titration experiment. Several experiments were conducted during method development and validation (data not shown) to determine apparatus assembly and equipment settings to ensure sufficient solution mixing during titrant addition. A diagram of the titration apparatus setup, with an accompanying picture of the actual cuvette assembly, is shown below in Figure 1.

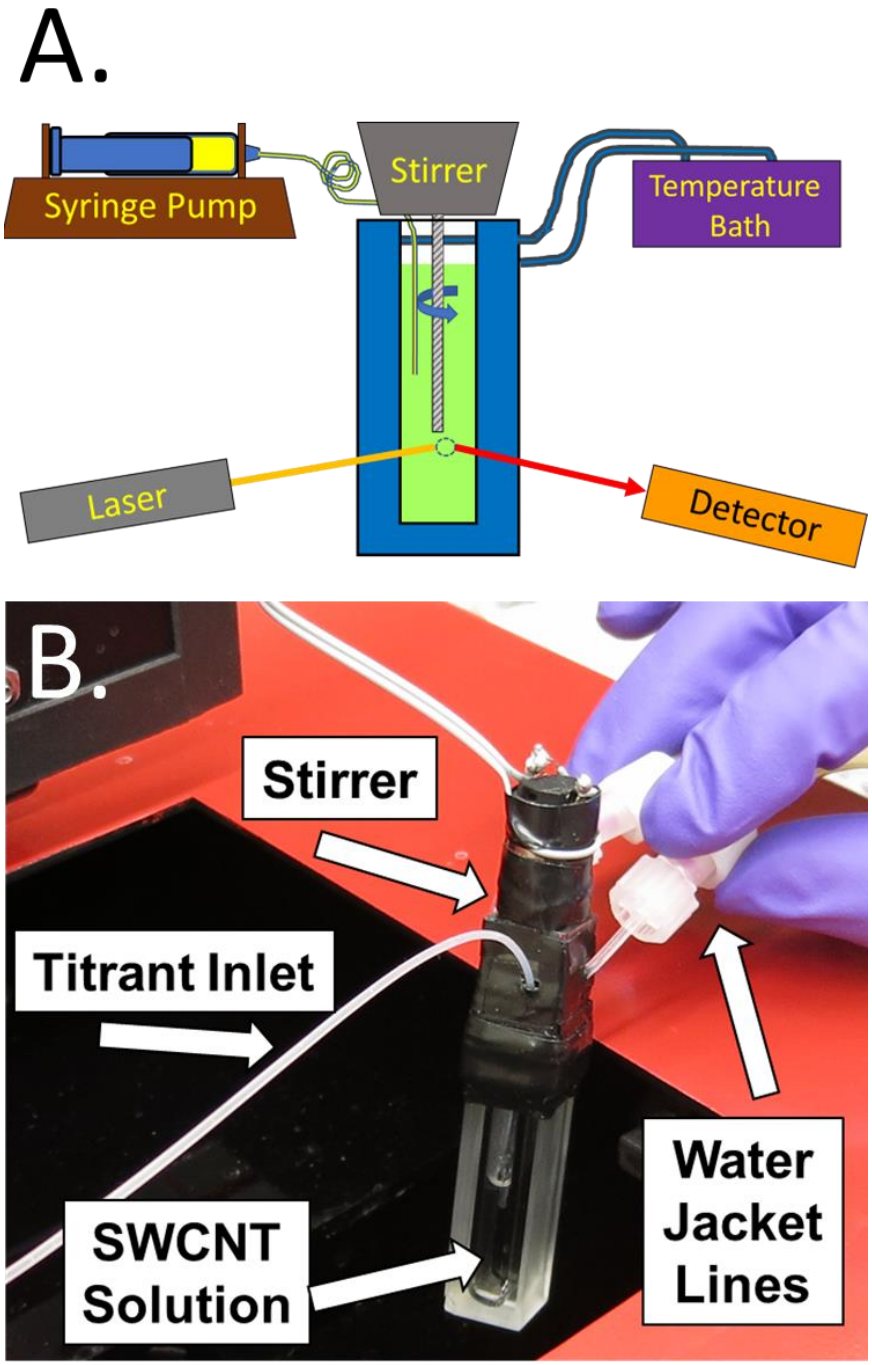

Figure 1. A) Schematic of the automated gradient titration setup housed within the fluorescence spectrophotometer. A stirrer provides rapid mixing of the SWCNT solution during titrant addition, while a temperature bath sets and maintains a fixed solution temperature. Fluorescence is measured in a front face collection geometry. B) Photograph of the actual cuvette assembly, with titrant inlet, stirrer, and water jacket temperature control lines noted.

NIR fluorescence detection acquisitions were set at 3 × 250 ms, with the SWCNT concentration set to be sufficiently low to limit detector counts to within the linear range of the NIR detector array

under all conditions. Unless otherwise noted, automated acquisition of fluorescence data was set to be acquired every 9.6 s during the titration, which when combined with the titrant addition rate (20 μL/min), means that 3.2 μL of titrant is added between each data point under typical experiment conditions. The peak fluorescence emission wavelength depends on the SWCNT species and were ≈ 1032.5 nm for (7,5) and ≈ 1125 nm for (8,4). Given that the (7,5) was the primary species in the sample, 637 nm excitation data was used for all data plots. The observed intensity at each timepoint was linearly corrected for the simultaneously recorded laser power and the dilution factor of the nanotube concentration due to the known added titrant volume; after point corrections were applied, the entire data set is then scaled by the maximum observed intensity (= 10, Arb. Units) for the data set, which typically resulted from the (7,5) signal (≈ 1032.5 nm). The resultant data are generally shown as scaled fluorescence intensity *versus* SDS concentration plots at the wavelength of peak E_{11} emission for each respective (*n,m*) species.

Finite-width Heaviside functions were fit to the fluorescence intensity *versus* SDS concentration data to extract the PCCCs reported in the text and Tables S1-S3. The Heaviside fitting formula was taken from Agrawal et al. [30] and is shown in Equation 1.

$$I(c_{SDS}) = \frac{I_1+I_3}{2} + \left|\frac{I_1-I_2}{2}\right| erf\left(\frac{PCCC_1-c_{SDS}}{width_1}\right) + \left|\frac{I_2-I_3}{2}\right| erf\left(\frac{PCCC_2-c_{SDS}}{width_2}\right) \quad (1)$$

In Equation 1, c_{SDS} is the concentration of SDS, $I(c_{SDS})$ is the observed fluorescence intensity, and I_1, I_2, I_3, are the intensity of the initial plateau, intermediate plateau, and final plateau, respectively; $PCCC_i$ and $width_i$ are the partition coefficient change concentration (PCCC) and width of the i^{th} observed transition. For consistency with the separations literature, all PCCCs throughout the text are presented as mass/volume percentage of SDS in solution unless otherwise stated.

To better illustrate emission wavelength shifting due to surfactant binding effects, the fluorescence data are sometimes also shown as SDS concentration *versus* E_{11} fluorescence emission wavelength 2D contour plots, where the z-scale is the scaled fluorescence intensity. In these contour plots, the labeled dashed lines represent the wavelengths of peak E_{11} emission for the noted (*n,m*) species under the standard conditions [≈ 1032.5 nm for (7,5), ≈ 1125 nm for (8,4)] with peak-shifting due to surfactant interactions described as blue- or red-shifted with respect to these wavelengths.

Where specified, uncertainty in this contribution is reported as one standard deviation.

3. Results and Discussion

3.1 Optical Characterization of the (7,5)/(8,4)-enriched SWCNT Sample

Representative absorbance and fluorescence spectra of the (7,5)/(8,4)-enriched parent dispersion in 10.0 g/L DOC are presented in Figures 2A and 2B, respectively. Through absorbance measurements, the sample displays the characteristics of a high quality SWCNT dispersion [31], featuring sharp optical transitions and a large ratio of peak to background absorbance, as seen in previous reports [29, 32, 33]. Fluorescence data likewise result in strong emissions assignable to specific (*n,m*) species under excitation [34]. The feature sizes are different between the two techniques due to differences in the fluorescence cross-section of each (*n,m*) species at the chosen excitation wavelength (637 nm) [35]. Additional spectroscopic characterizations, namely 2D excitation-emission contour and circular dichroism (CD) data plots, for the sample are reported in Figures S1 and S2. Although multiple SWCNT species are present in the sample, presented fluorescence results will focus on the ≈ 1035 nm emission from the (7,5) species to simplify the presentation of data and discussion of experimental variables. The presence of other (*n,m*) SWCNTs are included by design, and utilized in later figures to demonstrate differential behavior due to the inclusion of additional solution components, and the capacity of the fluorescence-based method for multiplexed measurements.

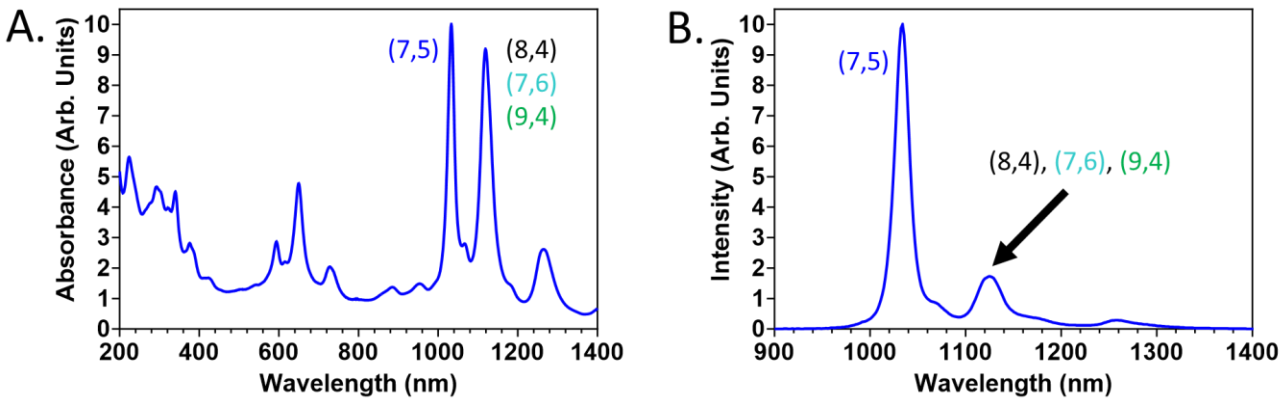

Figure 2. A) Absorbance spectra of the (7,5)/(8,4)-rich parent dispersion as measured in 10.0 g/L DOC. B) Fluorescence emission for dilute aliquots of the (7,5)/(8,4) rich parent dispersion at 637 nm excitation.

3.2 Validation of the Automated Gradient Titration Method

In our previous contributions [16, 22, 36], we monitored the fluorescence intensities of individually prepared SWCNT solutions with increasing SDS concentrations (at fixed 0.5 g/L (0.05 %) DOC and 35 g/L (3.5 %) 6 kDa PEG concentrations, hereafter referred to as "standard conditions") in a point-by-point manner. Representative (7,5) SWCNT fluorescence intensity data from the (7,5)/(8,4) sample using this approach is shown in Figure 3 (black diamonds). Increasing the SDS concentration (left to right) results in two distinct fluorescence intensity decreases, which represent the PCCCs for the two enantiomers of the (7,5) SWCNT under the experimental conditions; the naming convention is that the left-handed twist is the (7,5) and right-handed twist is the (5,7) [sometimes termed (12, -5)] respectively [37]. Although our previous approach offered quantitation for these PCCCs, improved precision in the determination of the PCCC values is of importance for situations where the PCCCs only vary by a small amount, such as enantiomeric pairs of certain (*n,m*)s [(7,6) for example], or where multiple species feature intertwined PCCCs (such as (7,5) and (8,4) as discussed further below).

To illustrate the improved resolution enabled by the developed automated gradient titration method, especially near the PCCC transition region, a gradient titration data set at the same standard conditions is also shown in Figure 3 (blue circles). That the new method provides a substantial increase in data density and hence, resolution is immediately apparent. Both PCCC transition regions are now covered by at least 7 data points (*versus* 1 before), facilitating a more accurate and precise quantitation of the PCCC values. These were calculated to be ≈ 0.688 % SDS and ≈ 0.747 % SDS for the two (7,5) enantiomers (denoted by dotted lines), which agree very well with previous literature results (Figure S3) [9, 16, 22, 23, 38]. As such, for the remainder of the text, we now simply display the individualized data points from the automated gradient titration method, with the Heaviside function used as a determinant of the PCCC values rather than included on top of the plotted data. The automated method also allows us to probe potential directionality-dependence in the transition in surfactant coverage at the PCCC point by reversing the direction of the gradient titration, *i.e.*, by titrating from greater SDS to lesser SDS concentration. We can now show, for the first time, that the surfactant exchange process is independent of direction and is free of hysteresis within, thus highlighting the consistent thermodynamics *and* kinetics of the surfactant competition (Figure 3, red squares). This observation further supports the proposed simple competitive surfactant adsorption mechanism as the underlying principle driving ATPE separations [15].

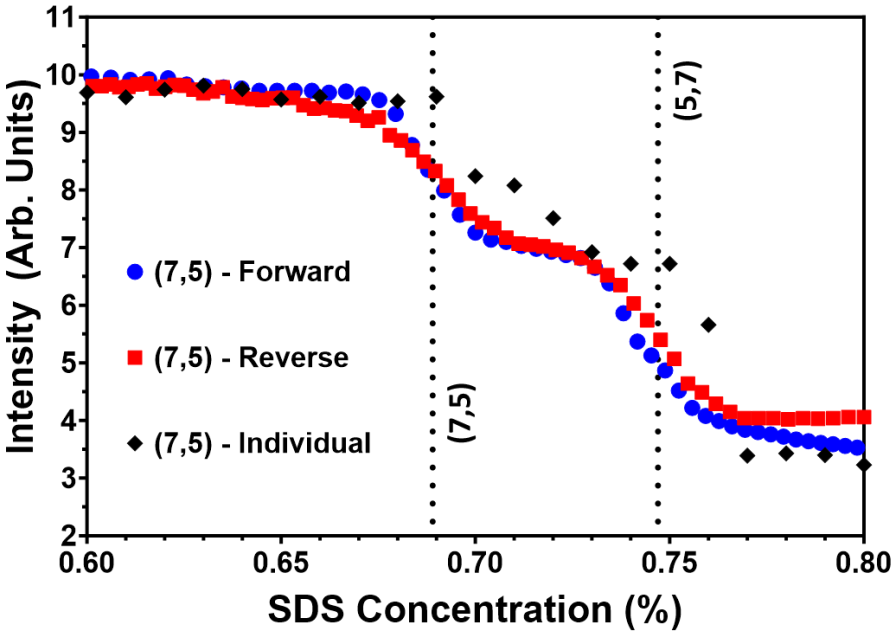

Figure 3. Fluorescence intensity of the (7,5) SWCNT for different experimental method variations as a function of the SDS concentration at a constant concentration of 35 g/L (3.5 %) PEG, and 0.5 g/L (0.05 %) DOC at 20.0 °C using the automated gradient titration setup. The fluorescence intensity curves overlap and yield the same PCCC values regardless of the titration direction: increasing SDS concentration (forward, blue circles) or decreasing SDS concentration (reverse, red squares). Data points from individually prepared solutions (black diamonds) are shown to illustrate the vast improvement in data density and resolution gained from the automated gradient titration method.

The increased data density and resolution of the automated gradient titration method not only enables more accurate determinations of the SWCNT (*n,m*) PCCCs, but also allows for the observation of previously unseen phenomena during the surfactant exchange process. Shown again in Figure 4a is a representative fluorescence intensity plot of the (7,5) SWCNTs as a function of SDS concentration under the standard conditions. With the automated method's increased resolution, we can now observe slight secondary inflections (denoted by the arrows in Figure 4a) where the rate of fluorescence intensity decreases deviates. Fascinatingly, these secondary inflections correlate with the calculated PCCC values at the exact midpoints of the transitions. This observation suggests that at the secondary inflection points during the transitions, there is a perturbation in the SWCNT-surfactant interaction, possibly attributable to rearrangement on the nanotube surface. To probe this anticipated perturbation in the surfactant shell, we now compare fluorescence spectra at five key points (shown in Figure 4b) during the

titration process: 1) the DOC-dominant region prior to the 1st PCCC (black); 2) the secondary inflection point during the 1st PCCC transition (blue); 3) the "plateau" in-between the two PCCCs (purple); 4) the secondary inflection point during the 2nd PCCC transition (red); 5) the SDS-dominant state region after the two PCCCs (orange).

Starting with the 1st region where DOC covers both (7,5) enantiomers, the fluorescence intensity is near the relative maximum (≈ 9.7, arb. units), with an emission wavelength of ≈ 1032.5 nm (noted in Figure 4b by the dotted line). At the 1st PCCC secondary inflection, the fluorescence intensity has decreased (≈ 8.0, arb. units), but the emission wavelength has now red-shifted ≈ 1.0 nm to ≈ 1033.5 nm. By the third region in between the two PCCS, the fluorescence intensity has slightly decreased (≈ 7.2, arb. units), with the emission wavelength now settled at ≈ 1034.5 nm, a net ≈ 2.0 red-shift relative to the initial value. At the 2nd PCCC secondary inflection, the emission wavelength now blue-shifts ≈ 1.0 nm back to ≈ 1033.5 nm with a correlated sharper intensity decrease (≈ 4.9, arb. units). Finally, in the SDS dominated region, the emission intensity is lower (≈ 3.7, arb. units) with an additional ≈ 1.0 nm blue-shift back to the initial ≈ 1032.5 nm emission wavelength. The corresponding full SDS concentration versus fluorescence emission wavelength 2D contour plot is shown in the SI (Figure S4).

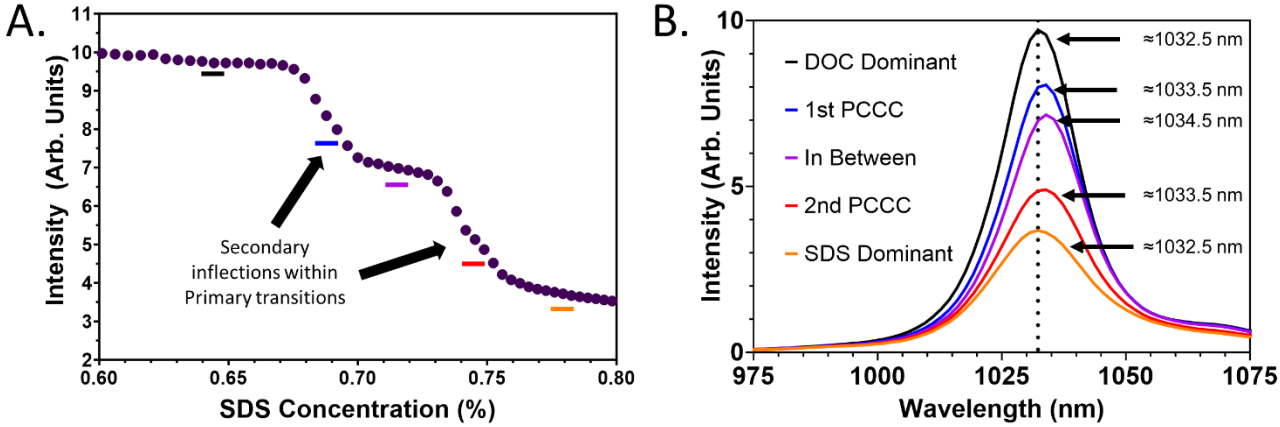

Figure 4. A) Fluorescence intensity of the (7,5) SWCNT as a function of SDS concentration at a constant 6 kDa PEG concentration of 35 g/L and constant 0.5 g/L DOC concentration at 20.0 °C. The color highlighted regions correspond to the B) fluorescence spectra of the sample taken at various points during the titration experiment. Note the presence of secondary inflections within the primary PCCC transitions in panel A and the shifting of the (7,5) emission wavelength during the titration experiment in panel B; the dotted line in panel B is at 1032.5 nm.

As shown in our previous contributions [16, 22] and elsewhere [17, 20, 21], replacing the initial SWCNT surface coating with a different surfactant can change not just the observed intensity (with which the PCCCs correlate), but can also shift the observed wavelength of fluorescence emission from the same (*n,m*) species. However, it is also known that the two enantiomers of the same (*n,m*) species can experience differences in their binding interactions with surfactants when those surfactants are also chiral [39-41], such as DOC (and other bile salt surfactants). In our experiments here, the observed fluorescence emission wavelengths were consistent at concentration regions in which *both* (7,5) enantiomers were expected to be dominated by either DOC (low SDS) or SDS (high SDS) coverage, with wavelength shifting only observable over the transition regions. This suggests the primary phenomena behind the wavelength shifting is the enantiomer-dependent differential binding of the surfactants, particularly the chiral DOC that (in typical experiments) initially covers the SWCNT-solution interface. With the knowledge that the 1st PCCC is assignable to the (7,5) enantiomer, we can assert that in the "plateau" region after the 1st PCCC point, the primarily DOC-covered (5,7) enantiomer is the greater contributor to the fluorescence signal, with the (7,5) enantiomer covered primarily by SDS and having relatively lesser fluorescence. However, the surfactant coating identity effect would presumably still contribute.

We also tested the robustness of the automated gradient titration method by varying the measurement and titration rates of the experiments. As described in the Methods section, under typical conditions, the titration rate is 20 µL/min with 9.6 s intervals in data acquisition, resulting in 3.2 µL of titrant addition between each data point. To probe any kinetic effects in the experiment, we tested increased measurement rates (*i.e.*, once per 4.8 s, 2.4 s, 1.2 s), with correlated increased titration rates (40 µL/min, 80 µL/min, 160 µL/min); note that in each case the titrant addition between points is the same, 3.2 µL. We compared these increased rate experiments, noted in Figure 5a as 2x, 4x, or 8x measurement rates to the typical conditions (noted as standard rate) for a representative experiment with the same experimental conditions and overall concentration gradient. As seen in Figure 5a, the agreement between all four conditions is practically quantitative, with only minor deviations seen in even the 8x rate experiment. These results demonstrate that the solution is sufficiently well mixed on the standard measurement time scale, while additionally serving to highlight the repeatability of the experiments and the possibility of increasing the experimental throughput beyond what is primarily

reported in this contribution. Being able to run the automated method even quicker will likely be important for accurate testing of kinetically sensitive effects, such as manipulation of the redox environment [15, 27].

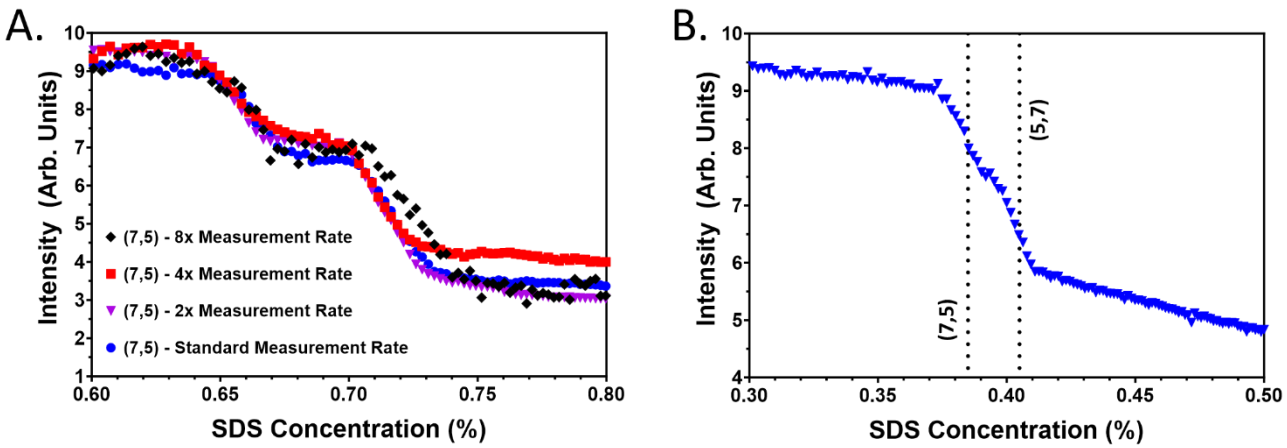

Figure 5. A) Fluorescence intensities of the (7,5) SWCNT as functions of SDS concentration at a constant 6 kDa PEG concentration of 35 g/L, with a constant DOC concentration of 0.5 g/L at 20.0 °C using the automated gradient titration setup. The fluorescence intensity curves overlap irrespective of measurement/titration rate. B) Fluorescence intensities of the (7,5) SWCNTs at constant DOC concentration of 0.5 g/L (0.05 %), in the absence of 6 kDa PEG, as a function of SDS concentration using the automated gradient titration setup at 20.0 °C. Note the reduced PCCCs in the absence of PEG.

Another benefit of the new automated titration method and its additional resolution is a much-improved applicability to thermodynamic analysis of the binding affinities of competing surfactants in solution. For most (*n,m*) species, resolution of such competitive binding was indeterminable within the previous point by point method experimental uncertainty for measurements in the absence of PEG [22]. Shown in Figure 5b is data from the automated method in the absence of PEG, in which the PCCCs of the two (7,5) enantiomers occur at significantly reduced (compared to standard conditions) SDS concentration. Although close together, distinct signals contributed from both (7,5) enantiomers are observed by the gradient method. This increased resolution should enable comparisons to and expansions of previous literature reports, since the DOC *versus* SDS system has been modelled by two-component isotherm models such as the Hill equation [39, 40, 42]. Although beyond the scope of this contribution, we anticipate forthcoming results to directly model the DOC/SDS surfactant pair competition for multiple (*n,m*) SWCNTs with resolution of their handed enantiomers.

It is also important to note of this methodology that the large degree of dilution possible for fluorescence experiments, combined with composition control of the titrant solution, enables either type of experiment described above to be trivially conducted in a D_2O solution environment if desired. Utilizing a D_2O environment improves observation of emission from larger diameter SWCNTs, and enables measurement of those *(n,m*) species emitting at wavelengths ≤ 1600 nm in our instrument. An example of an experiment conducted on a sample of such species is shown in the Supplemental Information as Figure S5.

3.3 Evaluation of ATPE Parameters *via* the Automated Gradient Titration Method

The dramatic increase in measurement speed and data density enabled by the automated gradient titration method most directly facilitates more efficient screening of ATPE parameters, especially combinations that would be very laborious to explore with physical separations. To demonstrate the automated methodology's capacity to screen the vast phase space of ATPE preparations more efficiently, we herein report initial studies on various three-component (DOC, SDS, 3rd component) systems to evaluate advanced parameter effects on SWCNT PCCCs. These experiments are chosen to demonstrate the potential of the new methodology for rapid screening and new exploration rather than intended as complete studies.

Due to the large phase space of potential ratios of combination, few studies have systematically explored three-surfactant competition systems for ATPE. One that has seen development consists of SDS, DOC, and the tri-hydroxy bile salt sodium cholate (SC) [25, 28, 36, 37, 43], this system has shown promise for improved separation of similar diameter SWCNT species and improved resolution of left- and right-hand twist enantiomers of some single species [(*n,m*) vs. (*m,n*)]. Figure 6 shows an example of screening the effects of adding a constant SC concentration to the DOC/SDS system in comparison to the standard condition run; titration curves are shown for both the (7,5) and the (8,4) species (blue circles and purple squares, respectively). It is immediately apparent that the addition of 9 g/L (0.9 %) SC significantly changes the SWCNT-surfactant interactions, as illustrated by the very different curve shapes and PCCC values for both species and their enantiomers (Figure 6, green triangles, and magenta diamonds, respectively). Changes to the SWCNT-surfactant interface perturbation are also illustrated by shifts in the emission wavelengths during the titration compared to the standard conditions (Figure S6).

Importantly, divergent behavior is observed for the shifts in the PCCCs of the two (*n,m*)s. Both (7,5) enantiomers shift to requiring higher SDS concentrations, with the magnitude of this shift varying for the two enantiomers, while the PCCCs for the (8,4) enantiomers are shifted to requiring *lower* SDS concentrations. In addition, the (8,4) curve also has a third fluorescence decrease (at ≈ 0.78 % SDS); we believe this transition is contributed by the small fraction of (7,6) or (9,4) SWCNTs in the sample. These species both have E_{11} emission wavelengths near that of the (8,4) (Figure S1). While we do not focus on it in this contribution, spectral deconvolution of fluorescence signals from mixed species populations is a goal of our future efforts.

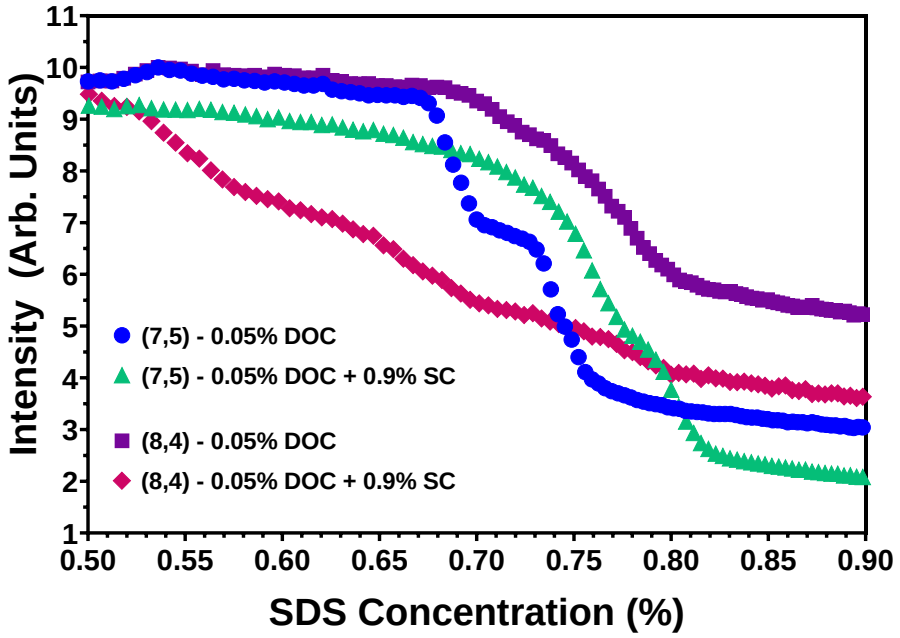

Figure 6. Fluorescence intensities of the (7,5) and (8,4) SWCNTs as functions of SDS concentration in the absence (blue circles and purple squares respectively) and presence (green triangles and magenta diamonds) of 9 g/L SC at a constant 6 kDa PEG concentration of 35 g/L, with a constant DOC concentration of 0.5 g/L at 20.0 °C. Importantly for separations, the addition of SC shifts the (7,5) PCCCs to higher SDS concentrations, while shifting the (8,4) PCCCs to lower SDS concentrations. PCCCs from Heaviside fitting are listed in Table S2.

It is well-known that SWCNT-bile salt interactions depend on several complicating factors; most importantly for the (7,5)/(8,4) sample discussed here, diameter and chiral angle [44]. While the (7,5) has a slightly narrower diameter than the (8,4), it features a larger chiral angle; these offsetting traits are illustrated in the empirical difficulty in separating the two species from each other (and supported by

their intermingled PCCC values as seen in Figure 6). However, the addition of SC resulted in a significant decrease in the (8,4) PCCCs concurrent with a slight increase in the (7,5) PCCCs, presumably yielding an overall ease of separating the two species using the three-surfactant DOC/SC/SDS mixture *versus* a two-surfactant mixture of SDS with either bile salt. Ascertaining the underlying physicochemical principles behind this effect is beyond the scope of this work, but a significant improvement in chirality sorting with such a three-surfactant system was also seen in work by Li *et al*., who used a DOC/SC/SDS mixture (of differing absolute concentrations) to isolate multiple species of SWCNTs with larger diameters than described here [25, 28]. As stated in those works, and discussed elsewhere [16, 36, 38], this improvement is thought to be dependent on the differences in surfactant coating owning to the slight structural differences between DOC and SC, namely the presence of the 7α hydroxy in SC affecting the bile salt electrostatics with further impacts on packing densities and thus susceptibility to replacement by SDS. While DOC is thought to be a stronger contributor to diameter-based sorting, SC is thought to have a greater sensitivity to chiral angle and enantiomeric handedness. However, when the two bile salts are used in tandem, the various influencing properties make it currently difficult to rank these competing preferences, As summarized in Li *et al*., ATPE separations of SWCNTs are extremely sensitive to subtle differences in surfactant coatings [28]. It is even possible from the intensity signal information only in this experiment that the order of (5,7) and (7,5) transition changed; other experiments have not found this to be the case for the (7,5) species with SC addition, but the possibility should be appreciated in performing broad surfactant combination and concentration phase space explorations. The preliminary data presented here represents an initial step toward a large enough data set to evaluate these complex interactions within these multi-surfactant ATPE systems, facilitating improved separations of different groups of (*n,m*) species. Such evaluations are ongoing and will be described in future contributions.

Another, almost completely unexplored, axis for modulating an ATPE system is the addition of an electrolyte component, such as NaCl [29, 45, 46]. Shown in Figure 7 are fluorescence intensity plots of the (7,5) as a function of SDS concentration under the standard conditions but increasing the concentration of NaCl. In the different runs, as the NaCl concentrations is increased, the PCCC values decrease. It was previously stated in Subbaiyan *et al*. that increasing the NaCl concentration in the ATPE system created a more favorable environment for SDS to compete with DOC [46] and our results agree with that observation. Notably, even though the absolute PCCC values decreased with increased NaCl

concentration, the presence of NaCl had no observable effect on the fluorescence emission wavelength of the (7,5) (Figure S7). This suggests that the addition of up to 50 mmol/L NaCl has no significant impact on terminal behavior of surfactant adsorption to the SWCNT surface, for either DOC *or* SDS. This compares very well with previous results from Duque *et al*., which noted no changes to DOC adsorption on SWCNTs at concentrations up to 40 mmol/L NaCl (with the DOC concentration held constant) [47]. Our observations are also consistent with Lam *et al*., which used analytical ultracentrifugation to determine that the anhydrous density of DOC-coated (7,6) SWCNTs in the presence of increased NaCl concentrations was constant at least up to 50 mmol/L NaCl; that observation implied that the SWCNT-DOC interactions were constant regardless of NaCl content [29].

As for why the PCCC values decrease, one hypothesis is that it could be coupled to the reduction in hydration shell thickness with ionic strength also previously measured for DOC coated SWCNTs by Lam et al. [3, 29] For SWCNTs, this shell is defined primarily by the bound layer of surfactant and its counter-ion cloud and is sufficiently structured by the electrostatic potential to exclude uncharged molecules, such as iodixanol used in the Lam *et al*. measurements, from approaching the SWCNT surface. Within the ATPE system, an increasingly shrunken hydration shell with increasing NaCl concentration would presumably allow for greater permeability of the anionic dodecyl sulfate groups to the SWCNT surface, potentially explaining the observed decrease in PCCCs.

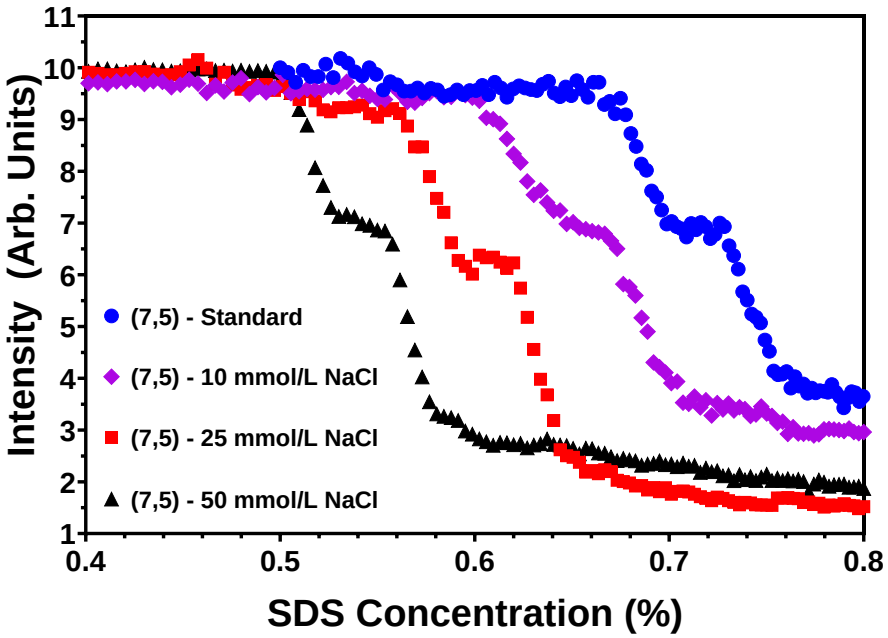

Figure 7. Fluorescence intensities of the (7,5) SWCNT as functions of SDS concentration for different concentrations of NaCl in the dispersion with a constant 6 kDa PEG concentration of 35 g/L and constant DOC concentration of 0.5 g/L at 20.0 °C. The amount of SDS necessary to change from a DOC-dominated interface to an SDS dominated interface decreases with increasing concentration of NaCl in solution. PCCCs from Heaviside fitting are listed in Table S3.

Having demonstrated the effects of salt concentration, it is an immediate and obvious question as to whether the specific anions and cations comprising any given electrolyte are observed to affect the PCCC values. Such a question is the focus of Figure 8, which shows a direct effect of the cation choice, and a lesser effect of anion choice for the shown traces; additional ongoing work beyond the scope of this contribution mostly follows such a trend, albeit with exceptions. In Figure 8 the fluorescence intensity is plotted for the (7,5) as a function of SDS concentration under the standard conditions, but with the inclusion of 25 mmol/L concentrations of other monovalent electrolytes (NaSCN and CsCl). The immediate observation is that the PCCCs of the NaSCN system is very similar to that of NaCl, while the PCCCs of the CsCl mixture are notably decreased compared to the NaCl mixture. Neither NaSCN nor CsCl appear to impact the fluorescence emission wavelength of the (7,5), a similar result as the NaCl experiments (Figure S8). That the presence of the salts doesn't cause a fluorescence shift may imply that the specific ion has little separate effect on the SWCNT-surfactant interaction, however, the differing

PCCC values and differences in fluorescence intensities during the titration suggest that there are surfactant-solution effects correlated with the identity and concentration of ions in the mixture.

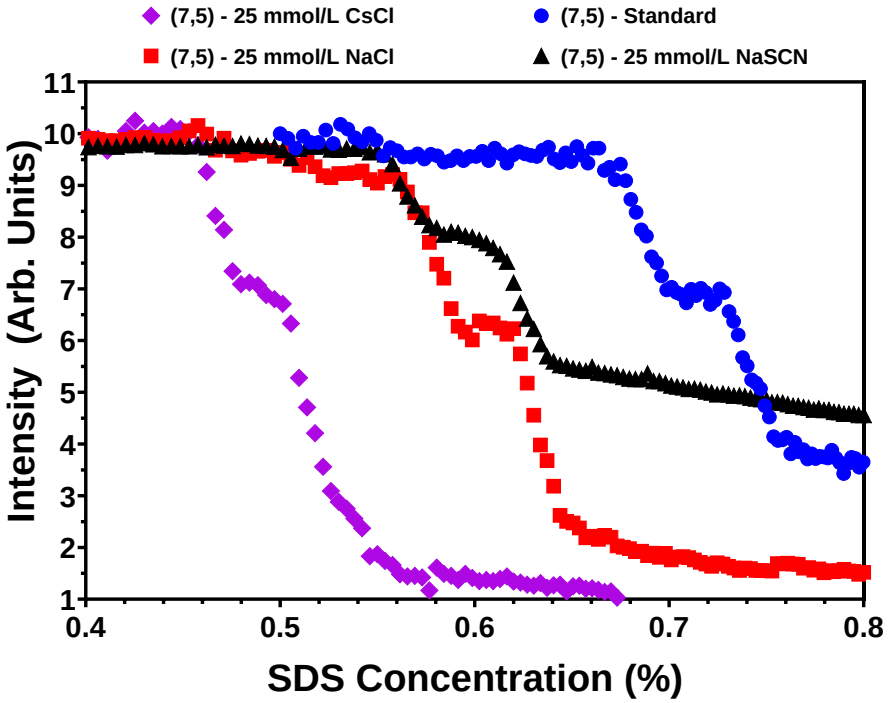

Figure 8. Fluorescence intensities of the (7,5) SWCNT as functions of SDS concentration with 25 mmol/L concentrations of different monovalent electrolytes in the dispersion with a constant 6 kDa PEG concentration of 35 g/L and constant DOC concentration of 0.5 g/L at 20.0 °C. The amount of SDS necessary to change from a DOC-dominated interface to an SDS dominated interface is impacted by the presence of electrolytes. PCCCs from Heaviside fitting are listed in Table S3.

Exploring anion *versus* cation effects, for the anion variation comparing the NaCl and NaSCN experiments, it is not surprising that the anion should have less of an impact on the observed PCCC values. While these anions are anticipated to contribute to the diffuse electrostatic double layer surrounding the SWCNT surface their incorporation is expected to be significantly less in the tightly bound layer at the SWCNT interface most likely to affect competitive binding. The reason for observation of the significant difference in reduction of the fluorescence intensity at the PCCCs for NaSCN experiment compared to the NaCl experiment is currently unknown; while Cl^- and SCN^- have the same ionic charge, their diameters, and thus other properties are different. Additional variation may elucidate the source

of this phenomenon. Interestingly for the cations the observed changes are effectively reversed. Comparing the NaCl and CsCl experiments, there is a significant difference (≈ 0.11 % SDS shift) in the measured PCCC values, but only a minor difference in the fluorescence intensity changes. Empirically, it appears that Cs^+ better enables dodecyl sulfate replacement of the initial DOC coating than Na^+. Previously, Duque et al. found that Cs^+ could associate with and bind a greater number of anionic dodecyl sulfate groups, which if applied here would presumably increase the localized concentration of dodecyl sulfate groups near the SWCNT surface and could explain the large decrease in PCCC values [47]. This rationale is further supported by Suttipong et al., whose results suggested that cesium dodecyl sulfate was a more effective (*i.e.*, stronger) SWCNT stabilizing agent than SDS [48]. That work also found that Na^+ being much smaller in size than Cs^+ (and consequently, having greater surface charge density) allowed it closer access to the SWCNT surface, with Cs^+ not being found in contact with the SWCNT surface. It should be noted that most of these previous studies on electrolyte effects on SWCNT optical properties were single surfactant (either DOC *or* SDS) studies, thus it is likely that any minor differences presented here are founded in the more complex mixed surfactant system in this work. Additional studies on the effects of various electrolytes on SWCNT sorting in the DOC/SDS system are ongoing and will be presented in future work.

4. Conclusions

In summary, we describe the development of a new automated titration fluorescence spectroscopy method for determining solution conditions leading to differential extraction of SWCNTs in ATPE systems. Compared to our previous method, the new setup results in significant increases in both the experimental throughput and resolution, while dramatically reducing the SWCNT sample required for experiments. These improvements help reveal previously unobserved complexities in the SWCNT-surfactant interface during the surfactant exchange process, while facilitating the evaluation of complex ATPE systems. Initial experiments on multi-component ATPE systems highlighted the ability to rapidly identify ATPE mixtures that could better isolate difficult to separate (*n,m*) species and their handed enantiomers. For the first time the effect of various monovalent electrolytes on SWCNT partitioning conditions in the mixed DOC/SDS ATPE system are reported. The addition of electrolytes is generally found to dramatically reduce the amount of SDS required to initiate PEG-phase partitioning,

with promising implications for ATPE scaling costs. Future work is expected to expand the screening of complex, multicomponent ATPE systems providing insights into new and unique types of ATPE-based SWCNT separations.

Acknowledgement

This effort was funded through internal National Institute of Science and Technology funds. The authors thank Paul F. Salipante and Steven D. Hudson of the NIST Materials Science and Engineering Division for their helpful suggestions and assistance on the automated titration setup.

Supplemental Information

The Supplemental Information contains additional spectroscopic characterization of the SWCNT sample (2D excitation-emission fluorescence contour plot and circular dichroism signal plots), surfactant concentration vs. fluorescence intensity contour plots, and data tables containing PCCCs as calculated from Heaviside fitting.

References

[1] F. Yang, M. Wang, D. Zhang, J. Yang, M. Zheng, Y. Li, Chirality Pure Carbon Nanotubes: Growth, Sorting, and Characterization, Chem. Rev. 120(5) (2020) 2693-2758.
[2] D. Janas, Towards monochiral carbon nanotubes: a review of progress in the sorting of single-walled carbon nanotubes, Materials Chemistry Frontiers 2(1) (2018) 36-63.
[3] M.S. Arnold, A.A. Green, J.F. Hulvat, S.I. Stupp, M.C. Hersam, Sorting carbon nanotubes by electronic structure using density differentiation, Nat. Nanotechnol. 1(1) (2006) 60-5.
[4] S. Ghosh, S.M. Bachilo, R.B. Weisman, Advanced sorting of single-walled carbon nanotubes by nonlinear density-gradient ultracentrifugation, Nat. Nanotechnol. 5(6) (2010) 443-50.
[5] H. Liu, D. Nishide, T. Tanaka, H. Kataura, Large-scale single-chirality separation of single-wall carbon nanotubes by simple gel chromatography, Nat. Commun. 2(1) (2011) 309.
[6] H. Liu, T. Tanaka, Y. Urabe, H. Kataura, High-efficiency single-chirality separation of carbon nanotubes using temperature-controlled gel chromatography, Nano Lett. 13(5) (2013) 1996-2003.
[7] C.Y. Khripin, J.A. Fagan, M. Zheng, Spontaneous partition of carbon nanotubes in polymer-modified aqueous phases, J. Am. Chem. Soc. 135(18) (2013) 6822-5.
[8] J.A. Fagan, C.Y. Khripin, C.A. Silvera Batista, J.R. Simpson, E.H. Haroz, A.R. Hight Walker, M. Zheng, Isolation of specific small-diameter single-wall carbon nanotube species via aqueous two-phase extraction, Adv. Mater. 26(18) (2014) 2800-4.
[9] J.A. Fagan, E.H. Haroz, R. Ihly, H. Gui, J.L. Blackburn, J.R. Simpson, S. Lam, A.R. Hight Walker, S.K. Doorn, M. Zheng, Isolation of >1 nm Diameter Single-Wall Carbon Nanotube Species Using Aqueous Two-Phase Extraction, ACS Nano 9(5) (2015) 5377-90.
[10] P.-Å. Albertsson, Partition of Cell Particles and Macromolecules in Polymer Two-Phase Systems, in: C.B. Anfinsen, J.T. Edsall, F.M. Richards (Eds.), Adv. Protein Chem., Academic Press1970, pp. 309-341.
[11] B.Y. Zaslavsky, Aqueous Two-Phase Partitioning: Physical Chemistry and Bioanalytical Applications, Marcel Dekker, Inc., New York, Basel, Oxford, 1995.
[12] N.K. Subbaiyan, A.N.G. Parra-Vasquez, S. Cambre, M.A.S. Cordoba, S.E. Yalcin, C.E. Hamilton, N.H. Mack, J.L. Blackburn, S.K. Doorn, J.G. Duque, Bench-top aqueous two-phase extraction of isolated individual single-walled carbon nanotubes, Nano Res. 8(5) (2015) 1755-1769.
[13] E. Turek, T. Wasiak, G. Stando, D. Janas, Probing the mechanics of aqueous two-phase extraction using large diameter single-walled carbon nanotubes, Nanotechnology 29(40) (2018) 405704.
[14] B. Podlesny, K.R. Hinkle, K. Hayashi, Y. Niidome, T. Shiraki, D. Janas, Highly-Selective Harvesting of (6,4) SWCNTs Using the Aqueous Two-Phase Extraction Method and Nonionic Surfactants, Advanced Science 10(14) (2023) 2207218.
[15] J.A. Fagan, Aqueous two-polymer phase extraction of single-wall carbon nanotubes using surfactants, Nanoscale Adv. 1(9) (2019) 3307-3324.
[16] C.M. Sims, J.A. Fagan, Surfactant chemistry and polymer choice affect single-wall carbon nanotube extraction conditions in aqueous two-polymer phase extraction, Carbon 191 (2022) 215-226.
[17] R. Haggenmueller, S.S. Rahatekar, J.A. Fagan, J. Chun, M.L. Becker, R.R. Naik, T. Krauss, L. Carlson, J.F. Kadla, P.C. Trulove, D.F. Fox, H.C. Delong, Z. Fang, S.O. Kelley, J.W. Gilman, Comparison of the quality of aqueous dispersions of single wall carbon nanotubes using surfactants and biomolecules, Langmuir 24(9) (2008) 5070-8.
[18] D. Roxbury, X. Tu, M. Zheng, A. Jagota, Recognition Ability of DNA for Carbon Nanotubes Correlates with Their Binding Affinity, Langmuir 27(13) (2011) 8282-8293.
[19] J.G. Duque, L. Oudjedi, J.J. Crochet, S. Tretiak, B. Lounis, S.K. Doorn, L. Cognet, Mechanism of electrolyte-induced brightening in single-wall carbon nanotubes, J. Am. Chem. Soc. 135(9) (2013) 3379-82.
[20] J.G. Duque, M. Pasquali, L. Cognet, B. Lounis, Environmental and synthesis-dependent luminescence properties of individual single-walled carbon nanotubes, ACS Nano 3(8) (2009) 2153-6.

[21] A.J. Blanch, J.G. Shapter, Surfactant concentration dependent spectral effects of oxygen and depletion interactions in sodium dodecyl sulfate dispersions of carbon nanotubes, J Phys Chem B 118(23) (2014) 6288-96.
[22] C.M. Sims, J.A. Fagan, Near -infrared fluorescence as a method for determining single -wall carbon nanotube extraction conditions in aqueous two polymer phase extraction, Carbon 165 (2020) 196-203.
[23] J. Defillet, M. Avramenko, M. Martinati, M.Á. López Carrillo, D. Van der Elst, W. Wenseleers, S. Cambré, The role of the bile salt surfactant sodium deoxycholate in aqueous two-phase separation of single-wall carbon nanotubes revealed by systematic parameter variations, Carbon 195 (2022) 349-363.
[24] B. Podlesny, B. Olszewska, Z. Yaari, P.V. Jena, G. Ghahramani, R. Feiner, D.A. Heller, D. Janas, En route to single-step, two-phase purification of carbon nanotubes facilitated by high-throughput spectroscopy, Sci. Rep. 11(1) (2021) 10618.
[25] H. Li, G. Gordeev, O. Garrity, S. Reich, B.S. Flavel, Separation of Small-Diameter Single-Walled Carbon Nanotubes in One to Three Steps with Aqueous Two-Phase Extraction, ACS Nano 13(2) (2019) 2567-2578.
[26] B. Podlesny, T. Shiraki, D. Janas, One-step sorting of single-walled carbon nanotubes using aqueous two-phase extraction in the presence of basic salts, Sci. Rep. 10(1) (2020) 9250.
[27] H. Gui, J.K. Streit, J.A. Fagan, A.R. Hight Walker, C. Zhou, M. Zheng, Redox sorting of carbon nanotubes, Nano Lett. 15(3) (2015) 1642-6.
[28] H. Li, G. Gordeev, O. Garrity, N.A. Peyyety, P.B. Selvasundaram, S. Dehm, R. Krupke, S. Cambre, W. Wenseleers, S. Reich, M. Zheng, J.A. Fagan, B.S. Flavel, Separation of Specific Single-Enantiomer Single-Wall Carbon Nanotubes in the Large-Diameter Regime, ACS Nano 14(1) (2020) 948-963.
[29] S. Lam, M. Zheng, J.A. Fagan, Characterizing the Effect of Salt and Surfactant Concentration on the Counterion Atmosphere around Surfactant Stabilized SWCNTs Using Analytical Ultracentrifugation, Langmuir 32(16) (2016) 3926-36.
[30] K.V. Agrawal, S. Shimizu, L.W. Drahushuk, D. Kilcoyne, M.S. Strano, Observation of extreme phase transition temperatures of water confined inside isolated carbon nanotubes, Nat. Nanotechnol. 12(3) (2017) 267-273.
[31] Y. Zheng, S.R. Sanchez, S.M. Bachilo, R.B. Weisman, Indexing the Quality of Single-Wall Carbon Nanotube Dispersions Using Absorption Spectra, J. Phys. Chem. C 122(8) (2018) 4681-4690.
[32] J.A. Fagan, M. Zheng, V. Rastogi, J.R. Simpson, C.Y. Khripin, C.A. Silvera Batista, A.R. Hight Walker, Analyzing surfactant structures on length and chirality resolved (6,5) single-wall carbon nanotubes by analytical ultracentrifugation, ACS Nano 7(4) (2013) 3373-87.
[33] C.A. Batista, M. Zheng, C.Y. Khripin, X. Tu, J.A. Fagan, Rod hydrodynamics and length distributions of single-wall carbon nanotubes using analytical ultracentrifugation, Langmuir 30(17) (2014) 4895-904.
[34] R.B. Weisman, S.M. Bachilo, Dependence of optical transition energies on structure for single-walled carbon nanotubes in aqueous suspension: An empirical Kataura plot, Nano Lett. 3(9) (2003) 1235-1238.
[35] J.K. Streit, S.M. Bachilo, S. Ghosh, C.W. Lin, R.B. Weisman, Directly measured optical absorption cross sections for structure-selected single-walled carbon nanotubes, Nano Lett. 14(3) (2014) 1530-6.
[36] H. Li, C.M. Sims, R. Kang, F. Biedermann, J.A. Fagan, B.S. Flavel, Isolation of the (6,5) single-wall carbon nanotube enantiomers by surfactant-assisted aqueous two-phase extraction, Carbon 204 (2023) 475-483.
[37] X. Wei, T. Tanaka, Y. Yomogida, N. Sato, R. Saito, H. Kataura, Experimental determination of excitonic band structures of single-walled carbon nanotubes using circular dichroism spectra, Nat. Commun. 7(1) (2016) 12899.
[38] M. Avramenko, J. Defillet, M.A. Lopez Carrillo, M. Martinati, W. Wenseleers, S. Cambre, Variations in bile salt surfactant structure allow tuning of the sorting of single-wall carbon nanotubes by aqueous two-phase extraction, Nanoscale 14(41) (2022) 15484-15497.
[39] M. Park, J. Park, J. Lee, S.Y. Ju, Scaling of binding affinities and cooperativities of surfactants on carbon nanotubes, Carbon 139 (2018) 427-436.
[40] H. Oh, J. Sim, S.Y. Ju, Binding affinities and thermodynamics of noncovalent functionalization of carbon nanotubes with surfactants, Langmuir 29(35) (2013) 11154-62.
[41] Y. Zhao, J.G. Clar, L. Li, J. Xu, T. Yuan, J.C. Bonzongo, K.J. Ziegler, Selective desorption of high-purity (6,5) SWCNTs from hydrogels through surfactant modulation, Chem. Commun. 52(14) (2016) 2928-31.

[42] S.Y. Ju, J. Doll, I. Sharma, F. Papadimitrakopoulos, Selection of carbon nanotubes with specific chiralities using helical assemblies of flavin mononucleotide, Nat. Nanotechnol. 3(6) (2008) 356-62.
[43] D. Yang, L. Li, X. Wei, Y. Wang, W. Zhou, H. Kataura, S. Xie, H. Liu, Submilligram-scale separation of near-zigzag single-chirality carbon nanotubes by temperature controlling a binary surfactant system, Sci. Adv. 7(8) (2021) eabe0084.
[44] S. Cambre, P. Muyshondt, R. Federicci, W. Wenseleers, Chirality-dependent densities of carbon nanotubes by in situ 2D fluorescence-excitation and Raman characterisation in a density gradient after ultracentrifugation, Nanoscale 7(47) (2015) 20015-24.
[45] S. Niyogi, C.G. Densmore, S.K. Doorn, Electrolyte Tuning of Surfactant Interfacial Behavior for Enhanced Density-Based Separations of Single-Walled Carbon Nanotubes, Journal of the American Chemical Society 131(3) (2009) 1144-1153.
[46] N.K. Subbaiyan, S. Cambre, A.N. Parra-Vasquez, E.H. Haroz, S.K. Doorn, J.G. Duque, Role of surfactants and salt in aqueous two-phase separation of carbon nanotubes toward simple chirality isolation, ACS Nano 8(2) (2014) 1619-28.
[47] J.G. Duque, C.G. Densmore, S.K. Doorn, Saturation of Surfactant Structure at the Single-Walled Carbon Nanotube Surface, Journal of the American Chemical Society 132(45) (2010) 16165-16175.
[48] M. Suttipong, N.R. Tummala, A. Striolo, C.S. Batista, J. Fagan, Salt-specific effects in aqueous dispersions of carbon nanotubes, Soft Matter 9(14) (2013) 3712-3719.